High variability in cross-shore thermally driven exchange

Hugo N. Ulloa[(1)], Kristen A. Davis[(2)], Geno Pawlak[(1)] and Stephen G. Monismith[(3)]

[(1)]Mechanical and Aerospace Engineering, University of California, San Diego, USA
[(2)]Civil and Environmental Engineering, University of California, Irvine, USA
[(3)]Department of Civil and Environmental Engineering, Stanford University, USA
hulloasanchez@eng.ucsd.edu

Abstract

The variability of cross-shore thermally driven exchange was examined using ensemble-averages of observations from the Kilo Nalu Observatory on the south shore of Oahu Hawaii. The cross-shore vertical shear, δV_z, top-bottom temperature difference, ΔT_z, and cross-shore advective heat flux, Q_{ex}, were analyzed to evaluate the influence of the surface heat flux, the cross-shore wind and the M_2 tide in the cross-shore exchange variability. The M_2 affects the exchange through the effects of tidally driven alongshore flow on turbulent diffusivity and on Coriolis driven cross-shore accelerations. Lunar phase ensemble-averages are compared with a theoretical model to show that the interaction of the diurnal wind pattern and the tidally driven alongshore flow can lead to significant cross-shore exchange variability at sub-diurnal time scales.

1 Introduction

Nearshore physical processes can modulate the mass, momentum and heat transport in complex ecosystems such as coral reefs (Monismith, 2007). A key physical process in these environments is the cross-shore exchange, between nearshore and the adjoining ocean, because it regulates the transport of nutrients, phytoplankton and waste (e.g., Genin et al., 2009; Paul et al., 1997). Cross-shore exchange can be driven by a variety of mechanisms, including Ekman transport, buoyancy driven flows, cross-shelf wind driven surface currents, internal waves, and surface and internal tides, all of which have different spatial and temporal scales. The role of these various processes will depend on local characteristics, such as bathymetry, shelf width, stratification, etc (Monismith et al., 2006). In particular, field studies have identified that diurnal surface heat flux is an important mechanism in driving for cross-shore flows at diurnal time scale in coastal regions, where the bed depth increases toward offshore (Monismith et al., 1990, 2006; Molina et al., 2014). Here, the heat flux acting on the surface with a diurnal periodicity causes shallower waters to heat and cool more rapidly than deeper waters, thus setting up a cross-shore temperature gradient due to the change in depth. This thermal structure drives cross-shore baroclinic flow that exchanges momentum and heat between the reef and the adjoining ocean. The cross-shore flow pattern associated with the cooling/heating diurnal phase response is shown in schematic form in figure 1; the fluid response associated with the cooling phase (0-12 hr) leads to colder offshore flow at the bottom, balanced by warmer onshore flow at the surface, with the opposite flow pattern for the heating phase (12-24 hr) (Farrow, 2004; Monismith et al., 2006).

Field observations of the velocity and thermal structure at Kilo Nalu Observatory (KNO) on the south shore of Oahu, Hawaii show that thermally driven baroclinic exchange is a dominant mechanism for cross-shore transport for this tropical forereef environment, modulated principally by the diurnal surface heat flux signal, the wind speed/direction and tides (Molina et al., 2014). Velocity and temperature data were collected from a bottom mounted acoustic Doppler current profiler (ADCP, 1200 kHz RDI Workhorse) and a thermistor chain (T-chain, Precision Measurement Engineering Inc.) deployed at 12 m depth and 370 m from shore at KNO site during January to September of 2010. Local atmospheric data, including pressure, relative humidity, short wave radiation, air temperature, wind speed/direction were available for this period. Currents, tidal height and temperature data were averaged into 20 min ensembles and atmospheric data were averaged into 1 hr ensembles. The bathymetry slope at KNO is

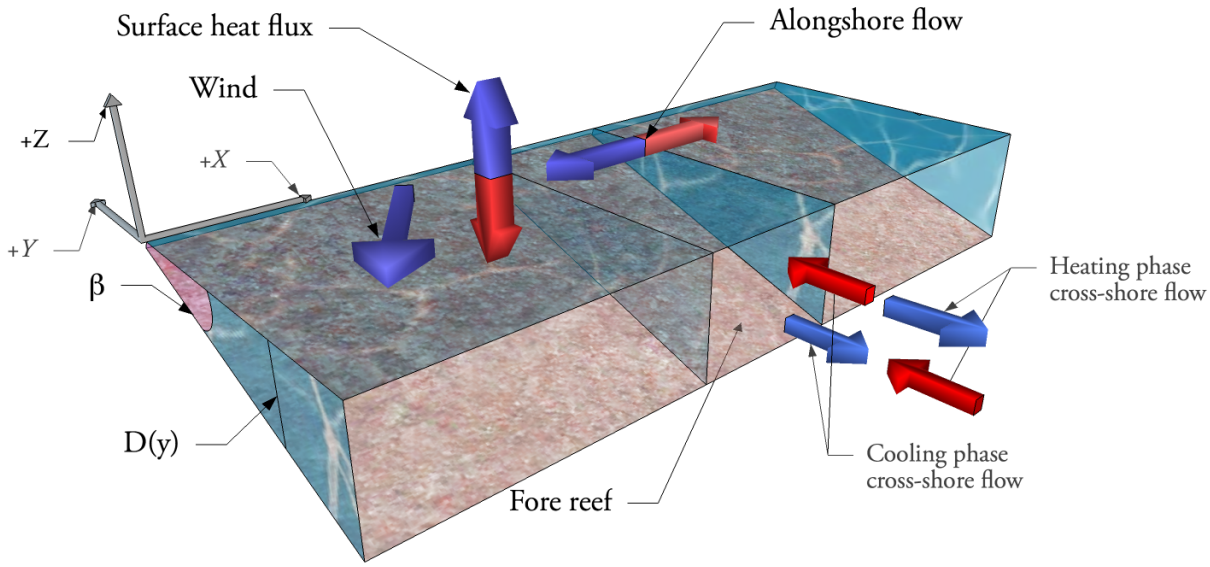

Figure 1: Schematic of the idealized fore reef system. Blue and red arrows mean negative and positive quantities respectively.

quite constant to the 20 m isobath 700 m from shore. Detailed information of the study site, instrument deployment and data processing can be found in Pawlak et al. (2009) and Molina et al. (2014).

Figure 2 shows the diurnal variation (vertical axis) of the main forcing mechanisms identified at KNO for 2010 (see Molina et al. 2014 for details). Net surface heat flux ($2a, b$) shows a robust diurnal pattern, characterized by a regular cooling phase and a heating phase; variations in magnitude are identified comparing winter and summer seasons. The cross-shore wind component ($2c, d$) shows a persistent offshore diurnal pattern, with a minimum in the early morning and a maximum during the afternoon. A few exceptional events associated with short onshore wind bursts, known as Kona storms, are observed during winter and fall months (positive winds in $1c$). Tide height ($2e$) drives alongshore flows, and its principal constituent is the semidiurnal M_2 (Pawlak et al., 2009). Figure $2f$ shows the tidal amplitude ensemble-averaged in terms of diurnal phase and M_2 phase. This result highlights the diurnal tide variation in terms of M_2 phase. The strength of the thermal exchange is reflected in the depth-averaged cross-shore shear over 3-10 m ($2g, h$) which has a marked diurnal profile (see figure $2h$). This diurnal flow pattern results from the dynamic regimes at KNO. Buoyancy conservation at KNO is dominated by an unsteady response while the momentum balance is largely between the baroclinic pressure gradient and turbulent diffusion (Molina et al., 2014). Although the thermally driven exchange has a robust diurnal structure in the long term, there is a high temporal variability on shorter time scales whose sources are not well understood.

In this study we investigate the role of the M_2 tidal phase and of the cross-shore wind in generating temporal variability in the thermal exchange at KNO. We consider an idealized three-dimensional wedge geometry, with a constant cross-shore slope β, to characterize a fringing reef environment (see figure 1). The system is periodically forced by a diurnal heat flux $H(t)$ that acts uniformly on the water surface. Additionally, the M_2 tidally driven alongshore flow and wind perturb the cross-shore momentum balance. The alongshore flow affects the cross-shore momentum balance indirectly via increased turbulent diffusivity and also through Coriolis accelerations. Hereinafter we assume that variations in buoyancy are only driven by variations in the thermal field. First, the exchange is analyzed via ensemble-averages of key measures of the cross-shore transport. Second, a three-dimensional theoretical framework is adopted to study the dynamic regime and the phase relationships observed for the KNO system.

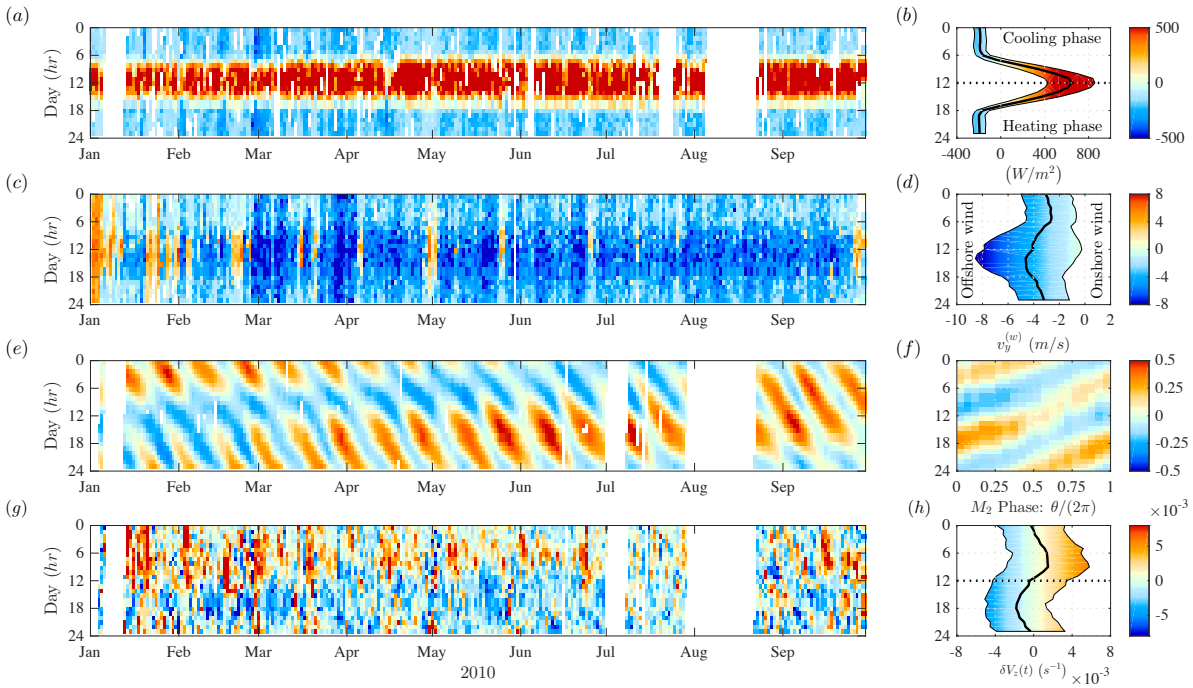

Figure 2: Observations at KNO for 2010. (a, c, e) diurnal variation of surface heat flux, cross-shore wind component and tidal amplitude, respectively. (b, d) diurnal variation of surface heat flux and cross-shore wind component, respectively, including their standard deviations. (f) tidal amplitude ensemble-averaged in terms of the diurnal profile and the M_2 phase. (g, h) depth-averaged cross-shore shear over 3-10 m.

2 M_2 phase variability

Two dominant time scales characterize the main forcing mechanisms, the solar day period, $\mathcal{T}_S = 24$ hr, for surface heat flux and wind, and the semidiurnal tide period, $\mathcal{T}_{M_2} = 12.42$ hr, for tidally driven alongshore flows. Although surface heat flux and wind have diurnal signals, they are shifted in phase. In addition, since the alongshore flow is dominantly forced at the M_2 frequency, its phase changes over a fortnightly cycle. Thermal exchange variability is studied in terms of three key measures, the average vertical shear, δV_z, the top-bottom temperature, ΔT_z, and the vertically averaged cross-shore advective heat flux, $Q_{ex} = \rho c_p \int_{-D}^{0} (v(z) - \langle v \rangle_D)(T(z) - \langle T \rangle_{LP})\, dz$, where ρ is the water density, c_p is the specific heat of water, D is the local depth, v is the cross-shore velocity component, T is the water temperature and $\langle T \rangle_{LP}$ is the depth-averaged low-frequency component based on a 66 hr cutoff.

Ensemble-averages of δV_z, ΔT_z and Q_{ex} were computed in terms of M_2 and solar phase. We use 20 bins to resolve the M_2 phase, in intervals of $\Delta\theta = \pi/10$ or 0.62 hr. Given the time window for the study (Jan-Sept. 2010) and the interval size, each ensemble is composed by 14 days $\pm$ 1 day. Solar time is resolved using 1 hr ensembles.

Figure 3 shows ensemble-averages of δV_z, ΔT_z and Q_{ex} with tidal height contours overlaid. The three measures show a clear diurnal pattern associated with the thermally driven cross-shore flow, which implies $\delta V_z > 0$, $\Delta T_z \sim 0$ and $Q_{ex} > 0$ during response to the cooling phase (morning) and $\delta V_z < 0$, $\Delta T_z > 0$ and $Q_{ex} < 0$ during the response to the heating phase (afternoon/evening). However, high variability as a function of M_2 phase is evident. During the early cooling phase (0-6 hr in figure 3a, b, c) and the late heating phase (20-24 hr) δV_z, δT_z and Q_{ex} all show changes in flow patterns as a function of M_2 phase, as indicated by the changes in sign for each quantity. Changes are less evident during the late cooling phase (6-12 hr). The transition between cooling and heating phase (theoretically around 12 hr) is quite irregular in terms of M_2 phase, especially for ΔT_z. Although the ensembles are marked by significant variability, the three measures show a thermally driven pattern phase around mid

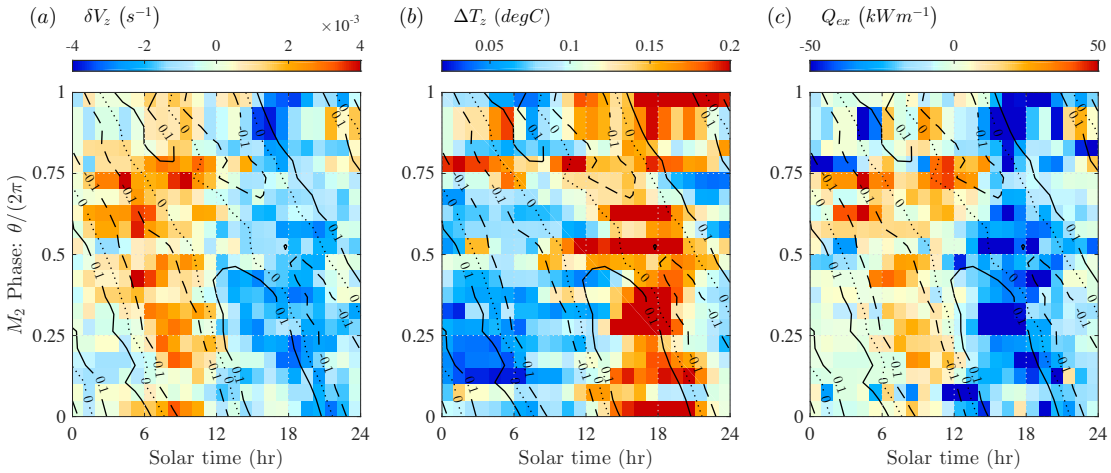

Figure 3: Ensemble-averages for vertical shear, δV_z, top-bottom temperature, ΔT_z, and vertically averaged cross-shore advective heat flux, Q_{ex} in terms of solar and M_2 phase. Contour lines show the ensemble-averaged tidal phase.

heating phase (16-20 hr). Variations in terms of M_2 phase suggest that alongshore flow is forcing and modulating the cross-shore exchange. The asymmetry that is evident between the cooling and heating responses suggests a role for the diurnal wind which is also characterized by an asymmetric profile. The role of the alongshore flow and cross-shore wind component in the cross-shore exchange pattern is investigated via the cross-shore momentum balance.

3 Theoretical model

Here we develop a theoretical approach focused on describing the forcing mechanisms that drive and perturb cross-shore flow at diurnal time scales. The natural time-scale is $t \sim \mathcal{T}_S$, which reflects the period for variations in surface buoyancy fluxes. We define the vertical length-scale by the local depth, $\ell_z \sim D(y)$; then, for a specific depth D, a suitable cross-shore length-scale is given by $\ell_y \sim \beta^{-1}\ell_z$. Additionally, we define an alongshore length-scale, ℓ_x, associated with the excursion of a periodic alongshore flow, assumed to be short enough to disregard alongshore velocity gradients, $\partial\vec{v}/\partial x \sim 0$.

Velocity components can be scaled as $u \sim U_0$, $v \sim V$ and $w \sim W$, where U_0 is the alongshore velocity scale associated to tide driven flows, while v_b and w_b are the cross-shore and vertical velocity scales associated with the relevant dynamical balances. From the continuity equation, $\partial_y v + \partial_z w = 0$, it follows that $W \sim \beta V$.

Field observations (Molina et al., 2014) have shown that buoyancy at Kilo Nalu is governed by an unsteady balance,

$$\frac{\partial b^{(0)}}{\partial t} \sim \frac{\partial \mathcal{F}}{\partial z}. \tag{1}$$

where $\mathcal{F}$ is the buoyancy flux acting over the free surface. In the simplest case this can be modeled as $\mathcal{F}(t,y,z) = -\alpha g H(t)\delta(z)/(\rho_0 c_p)$, where α is the volumetric thermal expansion coefficient, $H(t)$ is the surface heat flux signal and $\delta(z)$ is the Dirac delta function. This balance has been adopted by Farrow (2004) to find a baseline or 'zero-order' cross-shore flow circulation. In this limit, we define the buoyancy scale as $b \sim \alpha g \Delta T_0 \sim g\alpha H_0 \mathcal{T}_s/(\rho_0 c_p D)$. Assuming a 'zero-order' hydrostatic balance, $\rho_0^{-1}\partial p^{(0)}/\partial z \sim b^{(0)}$, we can define a pressure scale associated to the cross-shore thermal gradient, $p \sim \rho_0 g \alpha \Delta T_0 D$.

Based on observations (Molina et al., 2014), we assume that the 'zero-order' cross-shore flow results from a balance between the baroclinic pressure gradient and the vertical momentum

diffusivity,

$$\frac{1}{\rho_0}\frac{\partial p^{(0)}}{\partial y} \sim \frac{\partial}{\partial z}\left(\nu_t^{(0)}\frac{\partial v^{(0)}}{\partial z}\right). \tag{2}$$

Hence, the horizontal velocity scale is given by $V \sim \beta\alpha g\Delta T_0 D^2/\bar{\nu}_t$, where $\bar{\nu}_t$ is a depth/time-averaged eddy viscosity. Note we consider that the unsteady term in the cross-shore momentum budget plays a secondary role.

From the scaling analysis described above, we adopt the following parameters to describe the dimensionless equations of motion:

$$Gr_t \equiv \frac{g\alpha\Delta T_0 D^3}{\bar{\nu}_t^2}, \quad Re_t \equiv \frac{U_0 D}{\bar{\nu}_t}, \quad Ro_b \equiv \frac{\mathcal{T}_f}{\mathcal{T}_S}, \quad \tan(\beta) \equiv \frac{\ell_z}{\ell_y}, \tag{3}$$

where Gr_t is a turbulent Grashof number, Re_t is a turbulent Reynolds number associated to alongshore flows, and Ro_b (buoyancy Rossby number) is the ratio between the local inertial time-scale, $\mathcal{T}_f$, and the horizontal buoyancy time-scale, $\mathcal{T}_s$. A large Ro_b number indicates that a system is dominated by buoyancy driven forces, while a small Ro_b number indicates that Coriolis force is important. However, the Coriolis effect will also depend on the ratio of the horizontal velocity scales, (U_0/V). Additionally, eddy diffusivity has been naturally scaled in terms of the vertical length-scale and the time scale, $\mathscr{D}_t \equiv \bar{\nu}_t/(D^2\ \mathcal{T}_s^{-1})$. Usually $\beta \ll 1$ so that $\tan(\beta) \approx \beta$, then terms multiplied by β^n, with $n \geq 1$, play secondary roles. Thus the equations of motion become

$$\frac{\partial\tilde{u}}{\partial\tilde{t}} + \mathcal{R}_u\left(\beta^1 Ro_b^{-1}, \beta^2, \beta^2 Gr_t\right) = -\frac{Gr_t}{Re_t}\left[\frac{\mathscr{D}_t}{\ell_x/D}\right]\frac{\partial\tilde{p}}{\partial\tilde{x}} + \mathscr{D}_t\frac{\partial}{\partial\tilde{z}}\left(\tilde{\nu}\frac{\partial\tilde{u}}{\partial\tilde{z}}\right), \tag{4a}$$

$$\frac{\partial\tilde{v}}{\partial\tilde{t}} + \mathcal{R}_v\left(\beta^2, \beta^2 Gr_t\right) = -\mathscr{D}_t\frac{\partial\tilde{p}}{\partial\tilde{y}} + \mathscr{D}_t\frac{\partial}{\partial\tilde{z}}\left(\tilde{\nu}\frac{\partial\tilde{v}}{\partial\tilde{z}}\right) - Ro_b^{-1}\left(\frac{U_0}{v_b}\right)\tilde{u}, \tag{4b}$$

$$\mathcal{R}_w\left(\beta^2, \beta^4 Gr_t\right) = -\mathscr{D}_t\frac{\partial\tilde{p}}{\partial\tilde{z}} + \mathscr{D}_t\tilde{b}, \tag{4c}$$

$$\frac{\partial\tilde{b}}{\partial\tilde{t}} + \mathcal{R}_b\left(\beta^2 Gr_t\right) = \frac{\partial\tilde{F}}{\partial\tilde{z}} + \frac{\mathscr{D}_t}{Pr_t}\frac{\partial}{\partial\tilde{z}}\left(\tilde{\kappa}\frac{\partial\tilde{b}}{\partial\tilde{z}}\right), \quad \frac{\partial\tilde{v}}{\partial\tilde{y}} + \frac{\partial\tilde{w}}{\partial\tilde{z}} = 0. \tag{4d}$$

Here $\sim$ denotes a dimensionless variable and $\mathcal{R}_u$, $\mathcal{R}_v$, $\mathcal{R}_w$ and $\mathcal{R}_b$ correspond to residuals of each equation in (4), which include terms multiplied by β^n, with $n \geq 1$, such as advective accelerations, the Coriolis acceleration in the alongshore momentum component and cross-shore momentum diffusion terms. The buoyancy equation (4d) incorporates a turbulent Prandtl number, $Pr_t = \bar{\nu}_t/\bar{\kappa}_t$. To obtain orders of magnitude for the parameters, we use average values observed by Molina et al. (2014) at KNO during 2010 at a depth of $D \approx 12$ m, $\beta \approx 3\times10^{-2}$, $Gr_t \approx 1.5\times10^3$, $\mathscr{D}_t \approx 9$, $Ro_b^{-1} \approx 0.7$ and $Ro_b^{-1}\,(U_0/v_b) \approx 1.8$. Here we have calculated the eddy viscosity as $\bar{\nu}_t \approx \kappa\bar{u}_\star h$, where κ is the von Kármán constant, $\bar{u}_\star$ is the bottom shear stress velocity associated with the horizontal flow (using a constant friction coefficient) and h is the mid-depth. It is important to note that $u_\star$ is strongly modulated by the alongshore bottom shear, which in turns is driven by the M_2 tide constituent. These numbers show that the unsteady inertial term and the Coriolis terms have the same order of magnitude and play second-order roles in the cross-shore momentum balance, supporting the observation by Molina et al. (2014) of a diffusive momentum/unsteady buoyancy dynamic balance as a baseline.

A baseline buoyancy field is obtained neglecting the residual terms $\mathcal{R}_{(\cdot)}$ and assuming an unsteady balance described by (1), with $H(\tilde{t})/H_0 = -\cos\left(2\pi\tilde{t}\right)$. Thus, the zero-order buoyancy field, $\tilde{b}^{(0)}$, is given by

$$\tilde{b}^{(0)} = \frac{\sin\left(2\pi\tilde{t}\right)}{2\pi\tilde{y}}. \tag{5}$$

This term forces the cross-shore pressure field that drives the cross-shore circulation. Neglecting the residual terms, $\mathcal{R}_{(\cdot)}$, the unsteady and Coriolis accelerations, and assuming a constant bulk

viscosity $\tilde{\nu} \sim \mathcal{O}(1)$, the baseline baroclinic/diffusive cross-shore flow is described by the cubic velocity profile derived by Farrow (2004):

$$\tilde{v}_{\nu}^{(0)} = -\frac{\tilde{y}}{96\pi}\left\{8\left(\frac{\tilde{z}}{\tilde{y}}\right)^{3} + 9\left(\frac{\tilde{z}}{\tilde{y}}\right)^{2} - 1\right\}\sin\left(2\pi\tilde{t}\right) \tag{6}$$

If we include the wind stress via a surface boundary condition, the solution can be written as a linear superposition of the baroclinic/diffusive buoyancy driven flow, $\tilde{v}_{\nu}^{(0)}$, and the wind driven flow, $\tilde{v}_{w}^{(0)}$ (Farrow, 2013), $\tilde{v}_{\nu,w}^{(0)} = \tilde{v}_{\nu}^{(0)} + \mathscr{W}_{\mathscr{B}}\tilde{v}_{w}^{(0)}$, where $\mathscr{W}_{\mathscr{B}} \equiv \left(A_{(w)}/\rho_0\right)\left(\beta g\alpha\Delta T_0 D\right)^{-1}$ is a dimensionless parameter quantifying the relative magnitude of wind surface stress to surface heat flux,

$$\tilde{v}_{w}^{(0)} = -\tilde{y}\left(\frac{\tilde{z}}{\tilde{y}} + 1\right)\left\{\tau_0/A_{(w)} + \sin\left(2\pi\tilde{t} - \phi_{(w)}\right)\right\}, \tag{7}$$

where $A_{(w)}$ is a stress wind amplitude, τ_0 is an onset wind stress and $\phi_{(w)}$ is the diurnal wind phase. The baroclinic/diffusive solution is used to obtain a 'first-order' correction of the cross-shore flow including the unsteady and Coriolis accelerations. Note that an unsteady perturbation term arises in the momentum balance as a result of the Coriolis term (associated with the tidally driven alongshore flow). In the hydrostatic limit, the first-order momentum equations are given by

$$\frac{\partial\tilde{u}^{(1)}}{\partial\tilde{t}} = -\frac{Gr_t}{Re_t}\left[\frac{\mathscr{D}_t}{\ell_x/D}\right]\frac{\partial\tilde{p}^{(1)}}{\partial\tilde{x}} + \mathscr{D}_t\tilde{\nu}\frac{\partial^2\tilde{u}^{(1)}}{\partial\tilde{z}^2}, \tag{8a}$$

$$\frac{\partial\tilde{v}^{(1)}}{\partial\tilde{t}} + \frac{\partial\tilde{v}_{\nu,w}^{(0)}}{\partial\tilde{t}} = -\frac{\partial\tilde{p}^{(1)}}{\partial\tilde{y}} + \tilde{\nu}\frac{\partial^2\tilde{v}^{(1)}}{\partial\tilde{z}^2} - Ro_b^{-1}\left(\frac{U_0}{v_b}\right)\tilde{u}^{(1)}. \tag{8b}$$

We consider an alongshore flow, $u^{(1)}$, driven by a barotropic M_2 tide pressure gradient over a no-slip boundary condition,

$$\frac{\partial\tilde{p}^{(1)}}{\partial\tilde{x}} = \sin\left(2\pi\frac{\omega_{M_2}}{\omega_{T_s}}\tilde{t} - \phi_{M_2}\right), \tag{9}$$

where ϕ_{M_2} is the M_2 phase. The solution of (8a) forced by (9) is the Stokes boundary layer flow

$$\tilde{u}_{M_2}^{(1)}\left(\tilde{t},\tilde{z}\right) = \cos\left(2\pi\frac{\omega_{M_2}}{\omega_{T_s}}\tilde{t} - \phi_{M_2}\right) - e^{-\tilde{k}_{\nu}(1+\tilde{z})}\cos\left(2\pi\frac{\omega_{M_2}}{\omega_{T_s}}\tilde{t} - \phi_{M_2} - \tilde{k}_{\nu}\left(1+\tilde{z}\right)\right). \tag{10}$$

where $\tilde{k}_{\nu} = \sqrt{\omega_{M_2}/(2\nu_t)}D$. Then, the first-order correction $\tilde{v}^{(1)}$ is numerically solved using both $\partial_{\tilde{t}}\tilde{v}_{\nu,w}^{(0)}$ and $\tilde{u}_{M_2}^{(1)}$ as source terms to obtain a new cross-shore velocity field $\tilde{v} \approx \mathscr{D}_t\tilde{v}^{(0)} + \tilde{v}^{(1)} + ...$ For this first-order solution, two cases are analyzed: (i) a constant bulk eddy viscosity $\bar{\nu}_t$ and (ii) an M_2 dependent eddy viscosity, $\nu_t(t) = \bar{\nu}_t(1 + \Delta_{\nu}|\tilde{u}_{M_2}^{(1)}|)$, where the term $\Delta_{\nu}|\tilde{u}_{M_2}^{(1)}|$ is used to recover the effective temporal structure of the alongshore flow. Wind and M_2 driven alongshore flow parameters were estimated based on field observations at KNO.

Theoretical solutions are compared using the top-layer cross-shore exchange velocity, $\langle\tilde{v}\rangle_{Tex} \equiv \langle\tilde{v}\rangle_{Top} - \langle\tilde{v}\rangle_{D}$, where $\langle\cdot\rangle_{Top}$ and $\langle\cdot\rangle_{D}$ represents the surface layer average and the depth average, respectively. This quantity has been previously used by Molina et al. (2014) to analyze the cross-shore momentum exchange. Figure 4 shows ensemble-averages of the theoretical top-layer cross-shore exchange velocity as a function of solar time and M_2 phase. Figure 4(a) shows the baseline top-layer cross-shore exchange velocity computed from equation 6, where we identify the diurnal and symmetric structure of a thermally driven flow only subject to diffusive momentum/unsteady buoyancy dynamic balance. The flow pattern transition (positive and negative exchange) occurs at 12 hr, in quadrature with the cooling/heating phase transition. Figure 4(b) shows results that includes the wind effect (see equation 7) over the baseline flow. In this

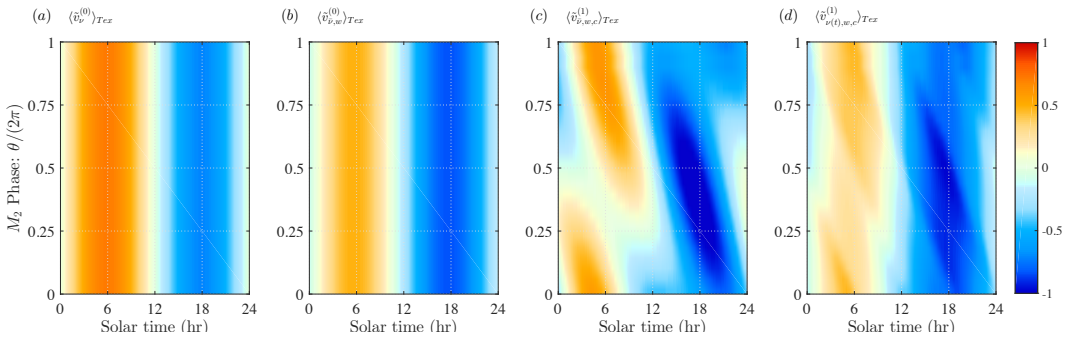

Figure 4: Ensemble-averages of theoretical top-layer cross-shore exchange for (a) baseline flow, $\langle\tilde{v}^{(0)}_{\bar{\nu}}\rangle_{Tex}$, (b) baseline/wind flow, $\langle\tilde{v}^{(0)}_{\bar{\nu},w}\rangle_{Tex}$, (c) unsteady/wind/Coriolis flow, $\langle\tilde{v}^{(1)}_{\bar{\nu},w,c}\rangle_{Tex}$, and (d) unteady/wind/Coriolis and time dependent eddy viscosity flow, $\langle\tilde{v}^{(1)}_{\bar{\nu}(t),w,c}\rangle_{Tex}$.

case, the superposition of the asymmetric average wind diurnal structure and the baseline cross-shore flow forces two changes in the top-layer cross-shore exchange. First, the diurnal top-layer exchange loses the symmetry so that the top-layer exchange is weakened during cooling phase and reinforced during heating phase. Second, there is a phase shift in the diurnal flow pattern transition. Figure 4(c) shows results that includes inertial and Coriolis accelerations in the top exchange flow. In this case, the flow solution shows a strong change with M_2 phase. The most evident change is in diurnal flow pattern transition and in flow magnitudes. There is a clear reinforcement of the offshore top-layer exchange during the heating phase, which can drastically change in terms of M_2 phase. In addition, the top-layer exchange flow shows changes in its flow pattern during the early cooling phase (0-3 hr) and the late heating phase (20-24 hr). Finally, figure 4(d) includes an M_2 time dependent eddy viscosity. This solution shows significant variability for both the heating and cooling phases in terms of M_2 phase, along with a more irregular diurnal transition flow pattern. Note that in this scenario three different cycles are involved, $\mathcal{T}_S$, T_{M_2} and $T_{M_2}/2$.

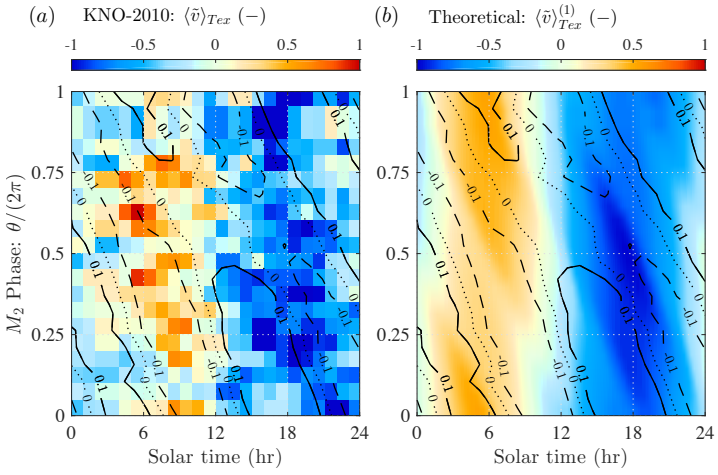

Figure 5: Ensemble-averages for (a) top-layer cross-shore exchange $\langle\tilde{v}\rangle_{Tex}$, and (b) theoretical top-layer cross-shore exchange, $\langle\tilde{v}^{(1)}_{\bar{\nu}(t),w,c}\rangle_{Tex}$ as a function of solar/M_2 phase. Quantities are normalized by twice the RMS variations for each. Contour lines represent tide amplitude.

4 Discussion

Ensemble-averages in figure 5 show the variation of the observed top-layer exchange velocity, $\langle\tilde{v}\rangle_{Tex}$, and the theoretical top-layer exchange velocity, $\langle\tilde{v}^{(1)}_{\bar{\nu}(t),w,c}\rangle_{Tex}$, as a function of solar time

and M_2 phase. The two quantities are normalized by twice their respective $RSM\,(\cdot)$ variations. The observations and perturbed solution show similar temporal patterns both in solar time and in M_2 phase. The cross-shore exchange shows a dominant diurnal profile but exhibits significant variability in terms of M_2 phase. Temporal variations in the cross-shore structure, $\langle \tilde{v}^{(1)}_{\bar{\nu}(t),w,c} \rangle_{Tex}$, derived from the theoretical analysis indicate that the main tidal constituent, M_2, plays an important role in the temporal variability observed at sub-diurnal time scales at KNO; tidally driven alongshore flows directly modulate the Coriolis exchange term but also perturb the effective eddy diffusivity, ν_t. Furthermore, the asymmetric response observed in the diurnal exchange pattern is explained in part by including the diurnal averaged variation in the cross-shore wind component, which weakens and reinforces the baroclinic flow response during the cooling and heating phase, respectively.

Although we have shown that variations in wind and alongshore flow can drive cross-shore exchange diurnal variability, substantial variability remains that is not well understood. Seasonal variations can change diurnal surface heat flux and diurnal winds, including via Kona storms. Secondary tide constituents can modulate alongshore flows and force asymmetries in the alongshore flow magnitude. In addition, lateral sources for warm or cold water can be driven by alongshore flows changing the thermal structure. Finally, intermittent physical processes, such as internal tides, bore excursions, wind driven baroclinic motions, etc, can enhance the high diurnal variability observed at the Kilo Nalu.

References

Farrow, D. E. (2004). Periodically forced natural convection over slowly varying topography. *J. Fluid Mech.*, 508:1–21, doi:10.1017/S002211200400847X.

Farrow, D. E. (2013). Periodically driven circulation near the shore of a lake. *Environ. Fluid Mech.*, 13:243:255, doi:10.1007/s10652--012--9261--4.

Genin, A., Monismith, S. G., Reidenbach, M. A., Yahel, G., and Koseff, J. R. (2009). Intense benthic grazing of phytoplankton in a coral reef. *Limnol. Oceanogr.*, 54(3):938–951, doi:10.4319/lo.2009.54.3.0938.

Molina, L., Pawlak, G., Wells, J. R., Monismith, S. G., and Merrifield, M. A. (2014). Diurnal cross-shore thermal exchange on a tropical forereef. *J. Geophys. Res. Oceans*, 119:6101–6120, doi:10.1002/2013JC009621.

Monismith, S. G. (2007). Hydrodynamics of coral reefs. *Annu. Rev. Fluid Mech.*, 39:37–55, doi:10.1146/annurev.fluid.38.050304..092125.

Monismith, S. G., Genin, A., Reidenbach, M. A., Yahel, G., and Koseff, J. R. (2006). Thermally driven exchange between a coral reef and the adjoining ocean. *J. Phys. Oceanogr.*, page doi:10.1175/JPO2916.1.

Monismith, S. G., Imberger, J., and Morison, M. L. (1990). Convective motions in the sidearm of a small reservoir. *Limnol. Oceanogr.*, 35(8):1676–1702, 10.4319/lo.1990.35.8.1676.

Paul, J. H., Rose, J. B., Jiang, S. C., P. London, X. X., and Kellogg, C. (1997). Coliphage and indigenous phage in mamala bay, oahu, hawaii. *Appl. Environ. Microbiol.*, 63(1):133–38, http://aem.asm.org/content/63/1/133.abstract.

Pawlak, G., de Carlo, E. H., Fram, J. P., Hebert, A. B., Jones, C. S., McLaughlin, B. E., McManus, M. A., Millikan, K. S., Sansone, F. J., Stanton, T. P., and Wells, J. R. (2009). Development, deployment, and operation of kilo nalu nearshore cabled observatory. *IEEE OCEANS*, page doi:10.1109/OCEANSE.2009.5278149.